



## OPEN ACCESS

## EDITED BY

Marinella Striccoli,  
Consiglio Nazionale delle Ricerche-CNR, Italy

## REVIEWED BY

Angsula Ghosh,  
Federal University of Amazonas, Brazil  
Urol Kudratovich Makhmanov,  
Academy of Sciences Republic of Uzbekistan  
(UZAS), Uzbekistan

## \*CORRESPONDENCE

Ana Paula de Carvalho Teixeira,  
✉ [anapct@ufmg.br](mailto:anapct@ufmg.br)

RECEIVED 16 March 2024

ACCEPTED 03 May 2024

PUBLISHED 21 May 2024

## CITATION

Diogo EBT, Vieira AFP, Nascimento MA,  
Pinto PS, de Paula FGF, Moreira RPL and  
Teixeira APC (2024), Carbon nanostructures  
supported on Co/serpentinite for  
sulfentrazone removal.  
*Front. Carbon* 3:1402105.  
doi: 10.3389/frcarb.2024.1402105

## COPYRIGHT

© 2024 Diogo, Vieira, Nascimento, Pinto, de  
Paula, Moreira and Teixeira. This is an open-  
access article distributed under the terms of the  
[Creative Commons Attribution License \(CC BY\)](https://creativecommons.org/licenses/by/4.0/).  
The use, distribution or reproduction in other  
forums is permitted, provided the original  
author(s) and the copyright owner(s) are  
credited and that the original publication in this  
journal is cited, in accordance with accepted  
academic practice. No use, distribution or  
reproduction is permitted which does not  
comply with these terms.

# Carbon nanostructures supported on Co/serpentinite for sulfentrazone removal

Emilay Baessa Teixeira Diogo<sup>1</sup>, Angelica Fonseca Pinto Vieira<sup>1</sup>,  
Mayra Aparecida Nascimento<sup>2</sup>, Paula Sevenini Pinto<sup>3</sup>,  
Fabiano Gomes Ferreira de Paula<sup>1</sup>, Renata Pereira Lopes Moreira<sup>4</sup>  
and Ana Paula de Carvalho Teixeira<sup>1\*</sup>

<sup>1</sup>Chemistry Department, Universidade Federal de Minas Gerais (UFMG), Belo Horizonte, Minas Gerais, Brazil, <sup>2</sup>Centro Federal de Educação Tecnológica de Minas Gerais (CEFET-MG), Belo Horizonte, Minas Gerais, Brazil, <sup>3</sup>Departamento de Ciências Naturais e da Terra, Universidade do Estado de Minas Gerais (UEMG), Divinópolis, Minas Gerais, Brazil, <sup>4</sup>Universidade Federal de Viçosa (UFV), Viçosa, Minas Gerais, Brazil

The presence of environmental contaminants is a major problem today. In this context, it is necessary to develop new sustainable materials to be used to remediate these contaminants. In this work, the serpentinite rock was impregnated with cobalt, 5%, 10% and 20% and used as a support for the synthesis of carbon nanostructures by CVD (chemical vapour deposition) process, at 900°C. This temperature was chosen due to the high thermal stability of the carbon source. The materials were characterized by X-ray diffraction, Raman spectroscopy, thermal analysis, scanning and transmission microscopy. As expected the main phases formed were forsterite, Mg<sub>2</sub>SiO<sub>4</sub>, graphitic carbon and metallic cobalt. All the synthesis showed the formation of carbon structures as multiwalled carbon nanostructures over cobalt cores. The carbon structures showed good thermal stability, between 470 and 600°C. The higher the cobalt content, the higher the yield of the carbon structures synthesis, i.e. 14%, 23% and 37% for Serp5, Serp10 and Serp20, respectively. The produced materials were used to removal of the environmental contaminant sulfentrazone. After CVD process, the removal of sulfentrazone increase to 17.3%, 18.4% and 25.2% for Serp5, Serp10 and Serp20, respectively, showing an increase in sulfentrazone removal with the increase in carbon content. In addition, the percentage of sulfentrazone removal by Serp20 was greater at acidic pH values, decreasing from 41.7% to 12.7% with an increase from 2 to 10 in pH. The removal capacity obtained experimentally at a sulfentrazone concentration of 50 mg L<sup>-1</sup> was equal to 14.9 mg g<sup>-1</sup>. According to literature and data obtained in this work, it was observed that the removal of contaminants from the aqueous medium occurred through two mechanisms: reduction of the organic compound by Co nanoparticles and adsorption carried out by carbon nanostructures.

## KEYWORDS

carbon nanostructures, serpentinite, chemical vapour deposition, adsorption, sulfentrazone

## 1 Introduction

Serpentinite is an ultrabasic rock that can be formed by silicate minerals: chrysotile ( $Mg_3(Si_2O_5)(OH)_4$ ), antigorite ( $Mg_3(Si_2O_5)(OH)_4$ ), lizardite ( $Mg_3(Si_2O_5)(OH)_4$ ), and talc ( $Mg_3Si_4O_{10}(OH)_2$ ) (Hirth and Guillot, 2013). Although the distribution and presence of these minerals depend on the place where this rock is present, serpentinite is basically a Si oxide tetrahedral sheet bounded to  $Mg(OH)_2$  based octahedral layer (Cao et al., 2017). Natural minerals, such as those based on serpentinite, are being increasingly used in environmental applications, due to their low cost, great abundance in nature, and easily obtainability (Lemos et al., 2016).

In this work, a novel approach was developed to use this natural inorganic material in removal of environmental contaminants, improving its properties by growing carbon nanofibers/nanotubes in its surface, producing amphiphilic materials. The CVD (Chemical Vapour Deposition) process is one of the most used for carbon nanotube synthesis based on technical simplicity, relatively low cost, and high yields (Purceno et al., 2011). Developed in the 1960s and 1970s, the CVD process consists of catalytic decomposition of carbon precursors (hydrocarbons, CO, alcohol) through catalysts, e.g., Fe/Mo, Ni, Co, that can be deposited on a thermally stable and preferably large surface area of an inert substrate (Dresselhaus et al., 2001; Dupuis, 2005; O'Connell and O'Connell, 2006; Öncel and Yürüm, 2006).

Previous work in our group has shown how those amphiphilic composites have special features. The simultaneous presence of hydrophilic Si and Si–Al oxide surface and hydrophobic carbon nanotubes (CNT) and nanofibers (CNF), allow the composites to interact well with aqueous and different organic phases. Furthermore, the presence of magnetic cores on the composite enables its removal from different media by a simple magnetic separation process (Teixeira et al., 2013; 2012; Purceno et al., 2012). These characteristics make amphiphilic materials interesting adsorbents for organic pollutants in aqueous media. One important class of organic contamination in wastewater is the herbicides.

The use of agrochemicals has grown rapidly due to high demand for food. However, the indiscriminate and disorderly use of these compounds may cause environmental and human health problems, such as gastrointestinal and respiratory system damages, cancer and fetal development issues, becoming a global concern (Siqueira and Kruse, 2008; Nascimento et al., 2016). Sulfentrazone is a pre-emergent herbicide and has a high potential persistence and moderate mobility in soil, and it may contaminate surface and ground water (Martinez et al., 2008). Therefore, the development of technologies that efficiently remove such substances becomes imperative.

Undabeytia et al. used clay-vesicle complexes composed of montmorillonite and positively charged didodecyldimethylammonium bromide (DDAB) mixed with clay (1:100 w:w) in a column filter to remove a solution with several organic pollutants in 10 mg/L initial concentration (Undabeytia et al., 2008). Their results were compared with sand/activated carbon filter. The best results were for anionic pollutants such Sulfentrazone and Imazaquin, achieving 100% adsorption capacity, but even the neutral ones (Alachlor and Atrazine) the results were three-fold higher for the clay-vesicle than the activated carbon filter. These results were achieved for 1 L solution. Lelario et al. also addressed the adsorption of organic pollutants (simazine, sulfentrazone and diclofenac) using a filter

filled with polymer-, micelle- and liposome-clay composite (Lelario et al., 2017). The authors found that high solubilization capacity was the major factor in sulfentrazone adsorption due to its hydrophobic nature and the best results were for the micelle-clay composite. These results show a potential for amphiphilic materials that could interact with both the aqueous solution and the hydrophobic pollutant decreasing the solubilization capacity factor.

In the literature, three publications were found on the use of serpentinite in adsorption processes. Momčilović et al. used serpentinite for the adsorption of  $Cd^{2+}$  and anionic organic textile dyes from synthetic water. Removals above 98% were achieved for  $Cd^{2+}$  and up to 99% for anionic dyes (Momčilović et al., 2016). Drizo et al. used serpentinite for the adsorption of phosphate from aqueous effluent. The results showed that serpentinite was efficient for removing 1.0 mg P/g in column studies (Drizo et al., 2006). Petrounias et al. activated serpentinite samples in a Los Angeles machine using different revolutions. And they observed that the materials obtained can be used as filters to remove  $Cu^{2+}$  from water (Petrounias et al., 2020). Although some papers have been published demonstrating the use of serpentinite in adsorption process, none have investigated its use in sulfentrazone removal, moreover, the potential combination of serpentinite and carbon nanostructures for that purpose.

Hereon, we described the synthesis of carbon nanofibers/nanotubes supported on serpentinite to produce magnetic amphiphilic composites to further investigate the removal of sulfentrazone contaminant in aqueous media.

## 2 Experimental

Serpentinite materials were provided by Pedras Congonhas Extração Arte Indústria (Nova Lima, Brazil). To study the changes in this mineral structure after a thermal treatment, the samples (5 g) were calcined at 800°C for 1 h in a tubular furnace using a quartz tube, with a heating rate of 10°C min<sup>-1</sup> and a flow rate of 50 mL min<sup>-1</sup> for different atmospheres: air and 8% H<sub>2</sub>/N<sub>2</sub> mixture. These samples were named Serp air and Serp H<sub>2</sub>, where Serp represents serpentinite.

### 2.1 Synthetic procedure

Serpentinite samples (5 g) were impregnated with an aqueous solution of cobalt nitrate hexahydrated in proportions of 5, 10 and 20 wt% of metal/support. The impregnation was done using 100 mL of cobalt nitrate hexahydrated at different concentrations in a beaker over magnetic agitation.

The resulting mixture was kept at 80°C, in a heating plate, until total evaporation of water. The obtained solids were further dried at 80°C during 24 h in a drying oven. The impregnated materials were reduced in a horizontal oven at 800°C (heating rate of 10°C.min<sup>-1</sup>) for 1 h in a H<sub>2</sub>/N<sub>2</sub> (8%) flow rate of 50 mL min<sup>-1</sup>. Then, the reduced materials were further heated at the same heating rate until 900°C for 1 h in 50 mL min<sup>-1</sup> flux of methane, using an alumina boat inside a quartz tube (CVD process). This temperature was chosen due to the high thermal stability of the carbon source. The materials were denoted as Serp5, Serp10, and Serp20, according to the cobalt content, wherein “Serp” denotes the name serpentinite, while 5, 10 and 20 refers the respective cobalt amount.

## 2.2 Characterization

The obtained materials were characterized by X-ray diffraction (XRD) using a Rigaku Geiger 2037 equipment,  $\text{CuK}\alpha = 1,54051 \text{ \AA}$  radiation,  $2\theta: 5^\circ\text{--}70^\circ$ ,  $4^\circ\text{.min}^{-1}$  with a copper tube); thermogravimetric analysis, using a DTG 60H model from Shimadzu, in air flow of  $50 \text{ mL min}^{-1}$ , heating rate of  $10^\circ\text{C.min}^{-1}$  until  $1,000^\circ\text{C}$ ; elemental analysis (carbon, hydrogen and nitrogen) were obtained using a Perkin Elmer 2,400 analyzer; Raman spectroscopy, using a model Senterra from Bruker, laser  $633 \text{ nm}$ ,  $2 \text{ mW}$ . 10 different measurements were taken, and the result was an average. A  $\times 50$  magnification objective was used to carry out the measurements, Scanning electronic microscopy (SEM), using a Quanta FEG 3D and Quanta FEG 200 equipments. For measurements, the samples were placed under a carbon tape; Transmission electronic microscopy (TEM), using a Tecnai G2-20 FEL. For measurements, the samples were dispersed in isopropanol and placed on holey carbon grids;  $\text{N}_2$  adsorption-desorption isotherm were obtained using a Quantachrome autosorb equipment. The isotherms were obtained at  $77 \text{ K}$ . Before the measurements, the samples were degassed at  $100^\circ\text{C}$  for 24 h.

## 2.3 Environmental applications

The prepared materials were used to remove the environmental contaminant, sulfentrazone. Initially, the adsorption equilibrium time between Serp5 and sulfentrazone was determined. For this,  $0.0100 \text{ g}$  of Serp5 were added to  $20.00 \text{ mL}$  of sulfentrazone solution at  $10.0 \text{ mg.L}^{-1}$ , under constant agitation and temperature, with aliquots removed at different time intervals. Subsequently, factors that may affect the sulfentrazone removal, such as cobalt content (5, 10% and 20%), pH (2, 4, 6, 8, and 10) and initial sulfentrazone concentration ( $5\text{--}50 \text{ mg.L}^{-1}$ ) were investigated. HCl and NaOH solutions, both at  $0.1 \text{ mol.L}^{-1}$ , were used to pH adjustment.

To describe the adsorption process, Langmuir and Freundlich isothermal models were used, Eqs (1), (2), respectively. The assays were performed using initial sulfentrazone concentrations of  $5\text{--}50 \text{ mg.L}^{-1}$ .

$$q_e = \frac{q_{\max} K_L C_e}{1 + K_L C_e} \quad (1)$$

$$q_e = K_F C_e^{1/n} \quad (2)$$

Wherein  $C_e \text{ (mg.L}^{-1}\text{)}$  is the sulfentrazone concentration at equilibrium,  $q_e \text{ (mg.g}^{-1}\text{)}$  is the amount of sulfentrazone adsorbed per Gram of adsorbent at equilibrium,  $q_{\max} \text{ (mg.g}^{-1}\text{)}$  is the maximum adsorption capacity,  $K_L \text{ (g.mg}^{-1}\text{)}$  is the constant Langmuir,  $K_F \text{ (mg.g}^{-1}\text{)}$   $\text{(mg.L}^{-1}\text{)}^n$  is adsorption capacity related constant and  $n$  is the constant related to adsorption intensity. In all assays, aliquots were removed from the system at pre-established times and filtered through nitrocellulose membrane ( $13 \text{ mm}$  of diameter and  $0.45 \mu\text{m}$  of porosity). The remaining sulfentrazone concentration was determined by High Performance Liquid Chromatography (LC 20AT Shimadzu) coupled to UV-Vis detector (SPD 20A Shimadzu) using C18  $150 \text{ mm} \times 4.6 \text{ mm}$  of internal diameter. The chromatographic conditions were: The mobile phase consisted of

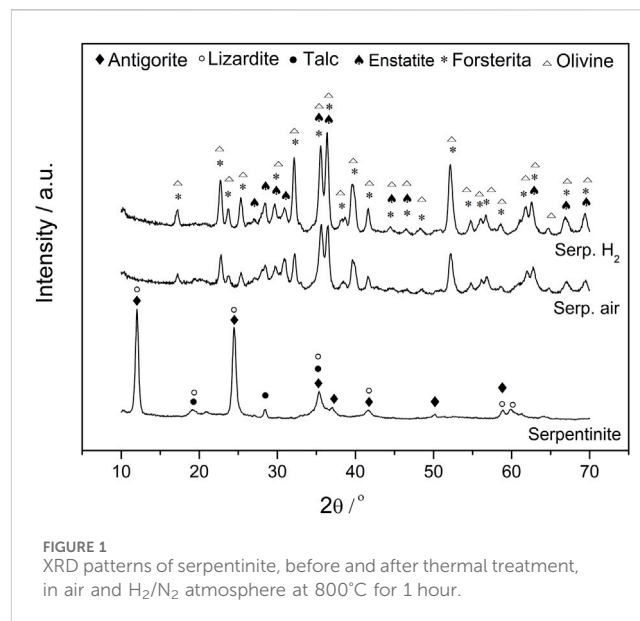


FIGURE 1  
XRD patterns of serpentinite, before and after thermal treatment, in air and  $\text{H}_2/\text{N}_2$  atmosphere at  $800^\circ\text{C}$  for 1 hour.

acetonitrile, ultrafiltrated water and phosphoric acid ( $50:49.9:1.1$ , v/v/v), injection volume  $20 \mu\text{L}$ , flow rate  $1.0 \text{ mL min}^{-1}$  and monitored wavelength was  $207 \text{ nm}$ .

The adsorption capacity  $q_e \text{ (mg.g}^{-1}\text{)}$  and removal rate (%) of sulfentrazone were calculated by Eqs (3), (4), respectively:

$$q_e = \frac{(C_0 - C_t)V}{m} \quad (3)$$

$$\% \text{ Removal} = \frac{(C_0 - C_t) \times 100}{C_0} \quad (4)$$

Wherein  $C_0$  is the initial sulfentrazone concentration and  $C_t$  is sulfentrazone concentration at time  $t$ ,  $V$  is the sulfentrazone solution volume and  $m$  is the mass of the material. All assays were performed in flasks coupled to a thermocriostatic bath (Microquímica, MQBTC 99–20) for temperature control.

## 3 Results and discussion

Before CVD process, the thermal stability of the serpentinite was studied at  $800^\circ\text{C}$  in both oxidant (air) and reducing ( $\text{H}_2/\text{N}_2$ ) atmosphere. Inert ceramic materials such as  $\text{MgO}$  and  $\text{Al}_2\text{O}_3$  are generally used as catalyst supports for the synthesis of carbon nanomaterials via the CVD process. These matrices are stable and do not decompose or undergo modifications during the carbon deposition process at high temperatures. Serpentinite is a natural material with hydroxyl groups that undergoes phase modification during the heating process. Furthermore, serpentinite contains  $\text{Fe}^{2+}$  and  $\text{Fe}^{3+}$  ions in its structure, which is why in this work we decided to carry out a preliminary study of this rock, both in an oxidizing and reducing atmosphere. This study helped us understand which active phases are present in serpentinite at high temperatures and to understand whether any oxidation or reduction process occurs in this material during heating.

The changes in structure were observed by XRD (Figure 1). The XRD patterns for serpentinite before thermal treatment showed

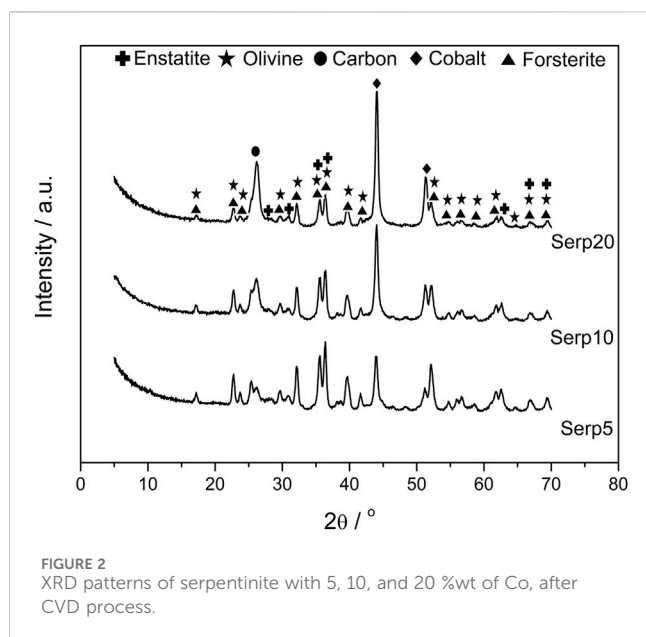


FIGURE 2  
XRD patterns of serpentinite with 5, 10, and 20 %wt of Co, after CVD process.

three minerals patterns, lizardite (JCDPS 18–779), antigorite ( $\text{Mg}_3\text{Si}_2\text{O}_5(\text{OH})_4$ , JCDPS 44–1,447) and talc ( $\text{Mg}_3\text{Si}_4\text{O}_{10}(\text{OH})_2$ , JCDPS 3–881), as constituents. Interestingly, no crysotile phase was observed and usually this silicate mineral is very common in serpentinite samples (Teixeira et al., 2013). After 800 °C treatment in air atmosphere, it can be noticed several changes in the XRD patterns after hydrate magnesium silicate phase modifications, yielding new mineral peaks characterized as forsterite ( $\text{Mg}_2\text{SiO}_4$ , JCDPS 34–189), olivine [ $(\text{Fe},\text{Mg})_2\text{SiO}_4$ , JCDPS 2–1,343] and enstatite ( $\text{MgSiO}_3$ , JCDPS 2–546) (Ballotin et al., 2016). There were no differences in mineral constitution in the serpentinite samples obtained after reducing atmosphere. But it was not possible more to observe the original phases from serpentinite rock at these temperatures. Consequently, we conclude that the phases presented during CVD process were forsterite, enstatite and olivine instead of the hydrated phases lizardite, antigorite and talc.

After understanding the actual mineral phases that will behave as support in the CVD process for CNS synthesis, serpentinite was impregnated with catalyst (Co) in three different metal/support ratios, named Serp5, Serp10 and Serp15 for 5, 10% and 15 wt of cobalt, respectively. The resultant materials were placed at 800 °C in  $\text{H}_2/\text{N}_2$  for catalyst reduction and then heated until 900 °C in  $\text{CH}_4$  for CNS growth. The temperature of 800 °C was chosen for the reduction of cobalt phases because, according to the literature, this value is sufficient for the formation of cobalt nanoparticles (Lemos et al., 2016).

In this work, it was decided to use a higher temperature in the carbon deposition process due to the carbon source used. According to previous work by the group and data from the literature, more stable sources of carbon such as methane and carbon monoxide require higher temperatures for their activation and decomposition. On the other hand, for less stable sources such as acetylene and ethylene, lower temperatures can be used (Shah and Tali, 2016; Silva et al., 2020; Teixeira et al., 2013; Tessonnier and Su, 2011). Figure 2 shows the XRD patterns for all materials after CVD process.

As expected, the XRD patterns showed non-hydrate silicate phases of forsterite, olivine and enstatite (as observed in Figure 1), for all materials. In addition, it can be observed new peaks related to the metallic cobalt (JCDPS 15–806) and graphitic carbon (JCDPS 1–640).  $\text{Co}^0$  was formed after the reduction step at 800 °C for catalyst activation, while graphitic carbon peaks indicate that carbon structures were formed in the CVD process. To elucidate the carbon structures, several techniques were used such as SEM, TEM, TG/DTG, elemental analysis, nitrogen isotherms at 77 K and Raman spectroscopy.

First, the impact of thermal treatment over the serpentinite structure was studied by SEM (Supplementary Figure S1, ESI†). Serpentinite showed a disperse structure with micrometric heterogeneous dimensions and morphology. The treatment at 800 °C in  $\text{H}_2/\text{N}_2$  atmosphere favoured the formation of some agglomerated particles, but no other significant change is observed. EDX analyses (Supplementary Figure S2, ESI†) for serpentinite showed the main presence of the elements Mg, Si, Fe and O. After heat treatments in oxidizing and reducing atmospheres, no change in the elements were observed. However, an increase in the relative intensity of the peaks referring to Mg and Si in relation to the peak of the oxygen element was noticed. This fact can be explained by the dehydroxylation of the hydrated phases of the serpentinite with loss of water molecules, which makes the phases richer in Mg and Si. After CVD process (Supplementary Figure S3, ESI†), the images show large agglomerates of carbon structures over the serpentinite support.

TEM images, Figure 3, enables a closer look at the carbon structures formed after CVD process. Most of the produced carbon is multi walled nanostructures with cobalt cores. Also, all catalytic systems were effective to grow these CNS, with no perceptible differences between the materials.

We used 12 different images of each material to carry out a statistical analysis of the diameter of the tubes and fibers formed. The results obtained were  $(43 \pm 12)$  nm  $(46 \pm 23)$  nm and  $(82 \pm 38)$  nm to Serp5, Serp 10, and Serp20, respectively. It is possible to observe that the standard deviation of the size of the structures was high, which can be justified by the heterogeneity of the structures formed and its relation to the natural support (serpentinite) used in the CVD process. Additionally, the higher the metal content used in the synthesis of the materials, the larger the diameter of the nanostructures produced.

According to the literature, there are two most common types of nanostructure growth mechanisms using the CVD process: “tip-growth” for large catalytic particles ( $\gg 5$  nm) and “base-growth” for smaller catalytic nanoparticles. From the TEM images it is possible to observe that the metallic nanoparticles inside the cavities of the carbon nanostructures have dimensions greater than 10 nm and smaller than 100 nm. Therefore, the possible mechanism for the CVD process in this work is based on tip-growth, with the formation of multiple carbon walls (Gohier et al., 2008).

The thermal stability measurements give us some information about the CNS organization structure and also about the yield of carbonaceous materials formed. The TG curves of the composites (Figure 4) showed a weight loss between 470 °C and 600 °C, related to CNS oxidation. The maximum oxidation temperatures were: 548 °C, 536 °C and 514 °C for the materials Serp5, Serp10 and Serp20, respectively. Meaning that an increase in cobalt amount

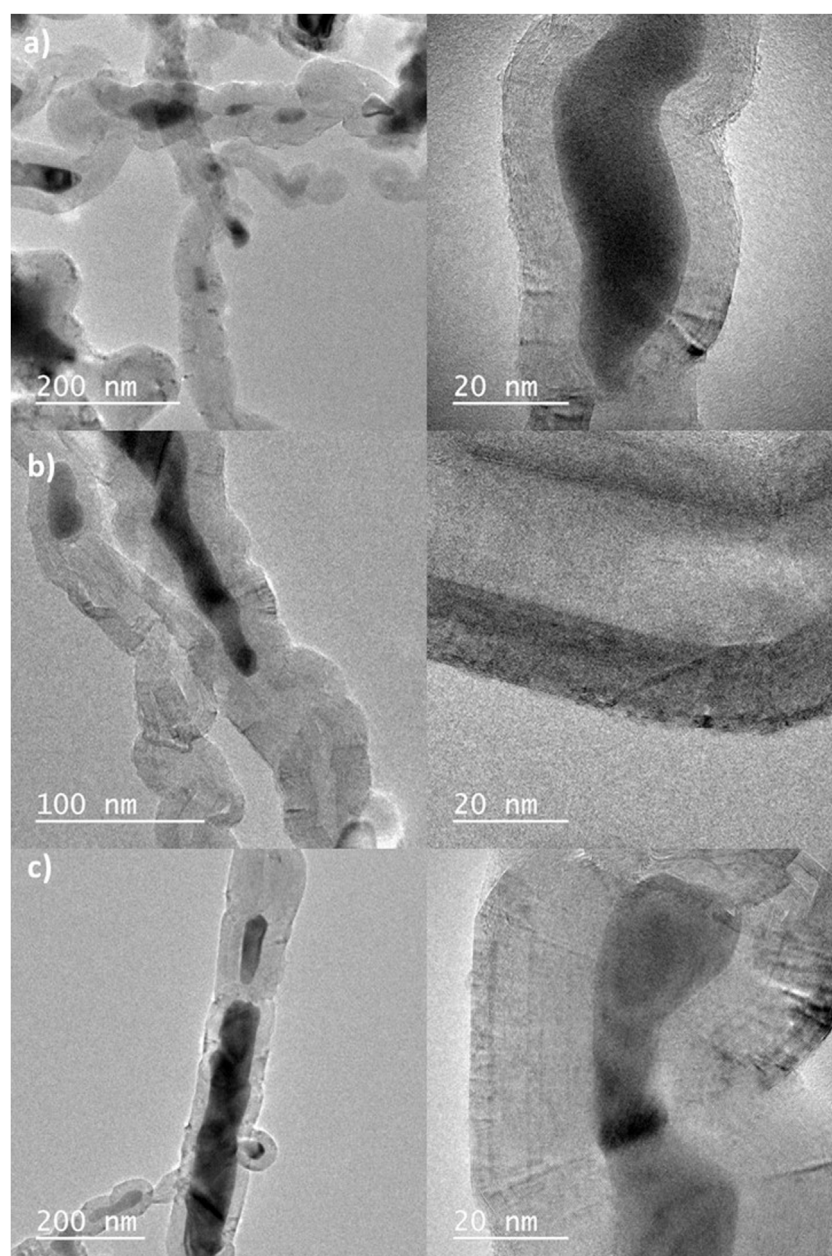


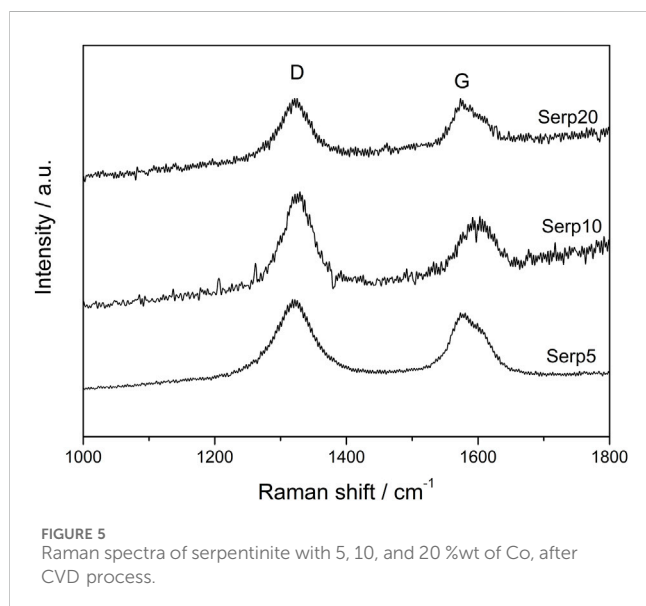
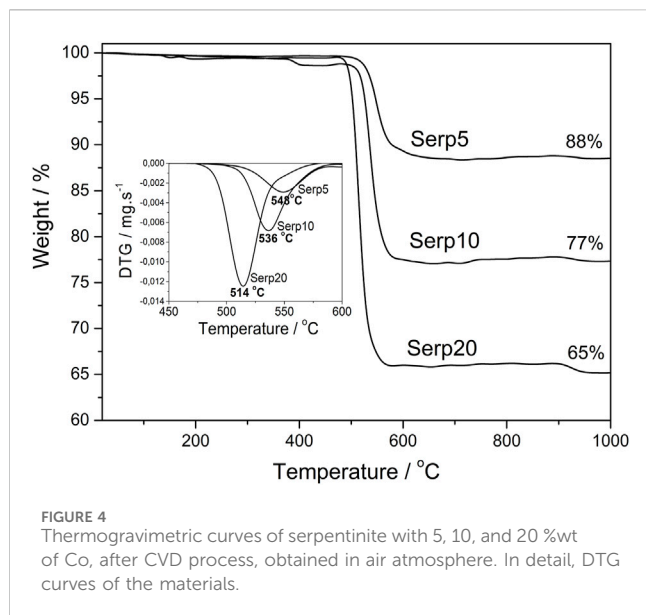
**FIGURE 3**  
TEM images of serpentine with 5 (A), 10 (B) and 20 (C) %wt of Co, after CVD process (methane 1 h).

promotes a decrease in the maximum oxidation temperature. There are two hypotheses that may justify this fact: i) higher Co content could favor the formation of less organized structures, such as amorphous carbon or carbon nanotubes with one or a few walls that is less stable; ii) the presence of large amounts of metal particles can also catalyse carbon oxidation, decreasing the maximum oxidation temperature (McKee and Vecchio, 2006). In all curves there were no loss weight events in low temperatures, which may indicate the absence of amorphous carbon in the materials (Zhao et al., 2011; Yang et al., 2012). Considering the weight loss, it was possible to determine the approximate amount of carbon present in each sample, being 12, 23% and 35% for Serp5, Serp10, and Serp20,

respectively. So, the higher the cobalt content, the higher the yield of the carbon structures synthesis.

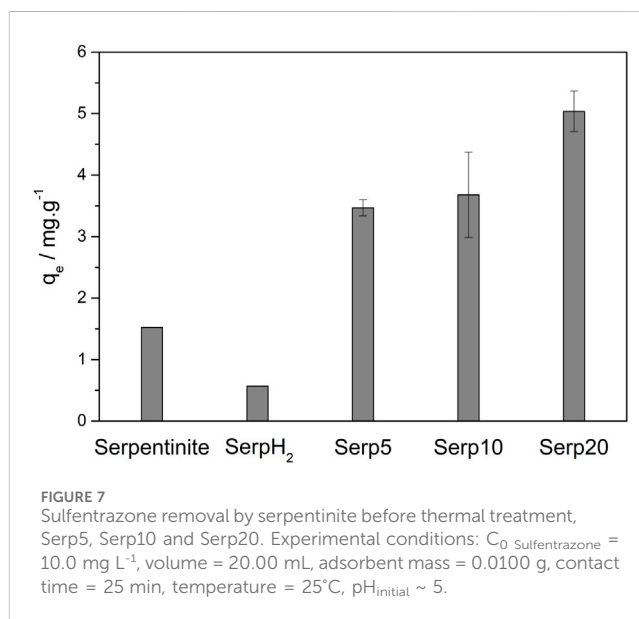
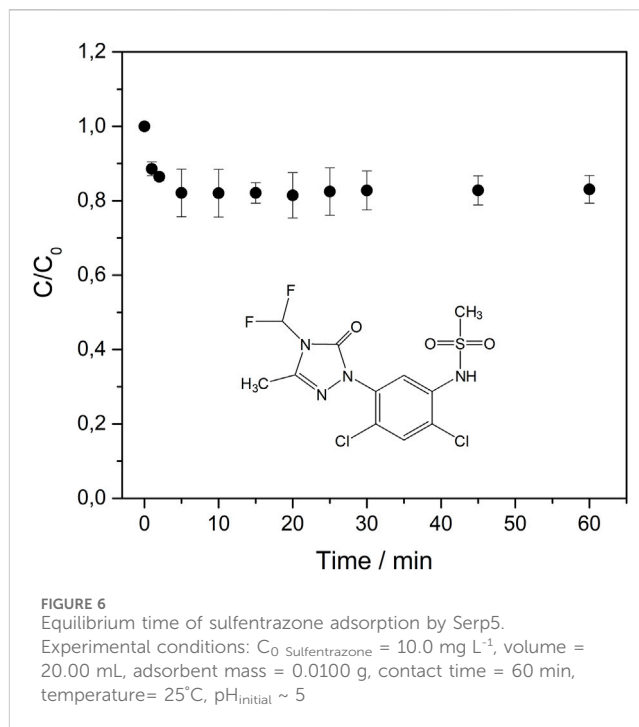
To confirm the carbon content of the materials, elemental analysis measurements were performed. As expected, the trend remained unchanged (14, 23% and 37 % wt, for Serp5, Serp10, and Serp20, respectively) and agreed with the obtained values by TG curves.

An important characteristic of adsorbent materials is its superficial area. Pure serpentine, as other natural minerals, has a low superficial area, i.e.  $10 \text{ m}^2 \text{ g}^{-1}$  (Cao et al., 2017). After nitrogen adsorption, the materials Serp5, Serp10 and Serp20 showed no significant difference in its superficial area, i.e. 7, 9 and  $14 \text{ m}^2 \text{ g}^{-1}$ ,



respectively. It would be expected some increase, comparing to pure serpentine, due to CNS formation, but in this case no significant change was noticed, probably due to an excess of serpentine (matrix) in the material.

For last, for further CNS structure elucidation, Raman spectra were obtained (Figure 5). Ten different measurements were carried out for each sample and all spectra presented here represents an average result. It is possible to observe the D and G characteristics bands for carbon materials, at 1,320 and 1,580  $\text{cm}^{-1}$  respectively (Figure 5). The D band refers to less organized carbon materials, generally defective structures, and the G-band is related to more organized carbon structures, i.e., graphite structures (Pimenta et al., 2007). The  $I_D/I_G$  ratio can be used as a parameter for the quality of carbon nanomaterials. The higher the ratio, the lower the structural



organization of the material (Beysac et al., 2003). The ratio values obtained were, 1.2; 1.1 and 1.0 to Serp5, Serp10 and Serp20, respectively. All values obtained were close to 1.0, which was expected as they were materials made from a natural support, with variable particle sizes, not favouring more organized structures. Again, no significant differences between the CNS of the three materials can be point out. Consequently, all techniques suggest that the Co content did not influenced the carbon structures, only the yield (increased when catalyst content was increased—Serp20).

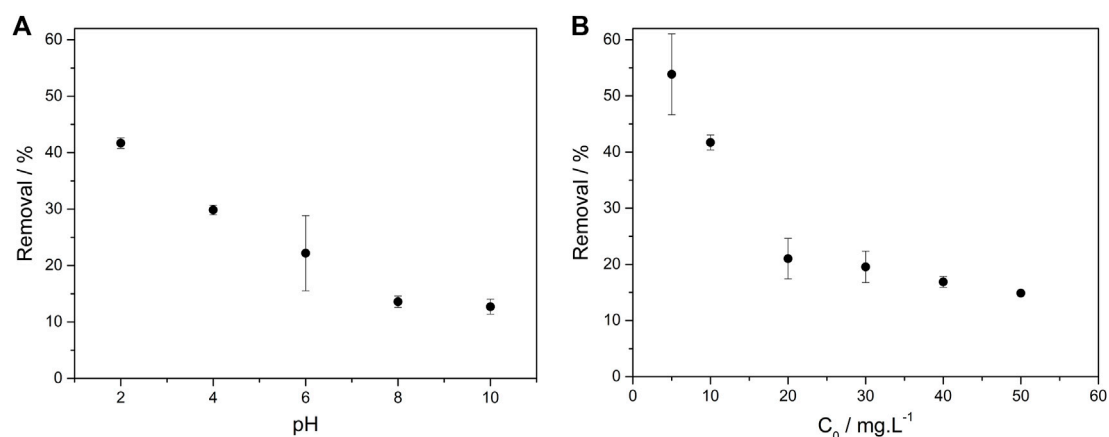


**FIGURE 8** Influence of initial pH (A) and initial concentration (B) on the sulfentrazone removal by Serp20. Experimental conditions:  $C_0$  Sulfentrazone = 10.0 mg L<sup>-1</sup> (A) and 5–50 mg L<sup>-1</sup> (B), volume = 20.00 mL, adsorbent mass = 0.0100 g, contact time = 25 min, temperature = 25°C,  $pH_{initial}$  = 2–10 (A),  $pH_{initial}$  = 2 (B).

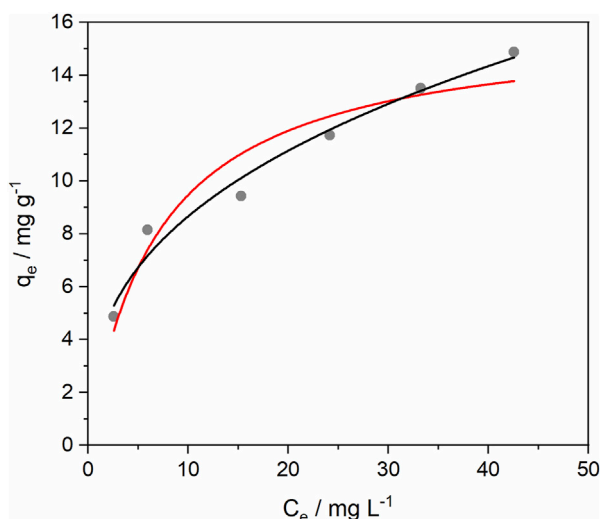


**FIGURE 9** Isotherm of Langmuir (—) and Freundlich (—) for sulfentrazone adsorption by Serp 20. Experimental conditions: Initial concentration 5.0–50.0 mg.L<sup>-1</sup>, solution volume 20.00 mL, adsorbent mass 0.0100 g, contact time 25 min, temperature 25°C, pH 2.

Our research group has been working on the synthesis of carbon nanostructures using natural minerals such as chrysotile (Lemos et al., 2016), vermiculite (Purceno et al., 2012) and mining waste (Silva et al., 2020) in the presence of iron or cobalt nanoparticles through the CVD process with different carbon sources and synthesis temperatures. Chrysotile, a silicate present in

serpentine rock, was impregnated with cobalt for the synthesis of carbon structures at temperatures between 600–900°C. It was observed that the best temperatures for synthesis were 800 and 900°C and the materials were efficient for adsorption of methylene blue dye (Lemos et al., 2016). Purceno and collaborators used the mineral vermiculite, a magnesium silicate, as a support for the deposition of iron and molybdenum nanoparticles. Then, it was synthesized nanostructures using methane as a carbon source at 800°C. The materials (~21% of carbon content) presented adsorption capacity between 2 and 4 mg m<sup>-2</sup> for the hormone ethinyl estradiol (Purceno et al., 2012). Iron mining tailings were used for the synthesis of carbon nanomaterials using ethylene and acetonitrile as carbon sources by the CVD process at temperatures between 500–900°C. The results obtained showed that higher temperatures led to the formation of carbon nanostructures with greater yield. The materials had a capacity to remove ethinyl estradiol hormone of up to 22.3 mg. g<sup>-1</sup> (Silva et al., 2020).

### 3.1 Removal of the sulfentrazone herbicide

The materials (Serp5, Serp10, and Serp20) were used to removal of the environmental contaminant sulfentrazone. As already discussed, this molecule is a pre-emergent herbicide and has a high potential persistence and moderate mobility in soil, which facilitates its accumulation and consequent soil and water contamination.

First, the equilibrium time required for sulfentrazone adsorption by Serp5 was determined, as shown at Figure 6. The sulfentrazone was rapidly removed by the material and 5 min were necessary for

**TABLE 1** Parameters of Langmuir and Freundlich for the sulfentrazone adsorption by Serp 20.

Langmuir			Freundlich		
$K_L/(L \text{ mg}^{-1})$	$q_m/(\text{mg g}^{-1})$	$R^2$	$K_F/(\text{mg g}^{-1}) (\text{mg L}^{-1})^n$	$1/n$	$R^2$
0.145 ± 0.046	16.0 ± 1.40	0.904	3.75 ± 0.424	0.364 ± 0.035	0.969

the concentration to remain constant. Initially, within the first 5 min, a larger number of active sites were available for adsorption. However, as time progressed, these active sites became progressively occupied, resulting in a deceleration of the adsorption process.

For the other experiments, it was chosen 25 min as reaction time, to obtain greater reliability that the equilibrium was reached despite any changed variable. All prepared materials and pure serpentinite were applied in the sulfentrazone removal, and the results are shown [Figure 7](#).

The removal of sulfentrazone by serpentinite prior to thermal treatment was 7.6%. This ability to remove sulfentrazone can be attributed to the presence of minerals such as antigorite, lizardite, and talc, as evidenced in the XRD results. These minerals have amphoteric hydroxyl groups, giving them an acid-base character that enables them to acquire an electrical charge contingent upon the pH of the system. Given that the pKa of serpentinite is 4.3 and that of sulfentrazone is 6.56, during the adsorption process (at pH~5), serpentinite becomes negatively charged while sulfentrazone carries a positive charge ([Alvarez-Silva et al., 2010](#); [Rodrigues and Almeida, 2018](#)). Consequently, an electrostatic attraction can occur, facilitating the adsorption of sulfentrazone. Similar findings were reported by [Momčilović et al.](#), who employed serpentinite for the adsorption of Cd(II) and anionic textile dyes ([Momčilović et al., 2016](#)).

After thermal treatment in reducing atmosphere, the sulfentrazone removal was only 2.8% in serpentinite. This occurred due the difference of minerals presents in the materials. Prior to thermal treatment, serpentinite presented phases of hydrated magnesium silicate, including antigorite, lizardite, and talc. However, following thermal treatment, the material exhibits phases of non-hydrated forsterite, olivine, and enstatite. These alterations in the mineral composition of serpentinite may result in a diminished electrostatic interaction between sulfentrazone and the materials, consequently leading to a reduction in adsorption capacity.

After CVD process, the removal of sulfentrazone increased to 17.3, 18.4% and 25.2% for Serp5, Serp10, and Serp20, respectively. The sulfentrazone removal increased with higher carbon content in the material. Carbonaceous materials, with  $sp^2$  hybridization, can promote the adsorption through  $\pi$ - $\pi$  interaction with the adsorbate aromatic ring ([Chen et al., 2021](#)). In addition, it could occur hydrogen bonding interaction between the sulfentrazone structure and the carboxyl group present in the materials. Thus,  $\pi$ - $\pi$  interaction, hydrogen bonding and electrostatic interaction may be responsible for the adsorption of sulfentrazone, in which led to a higher contaminant removal. [Duman et al.](#) also proposed that adsorption of the herbicide diquat dibromide by oxidized multi-walled carbon nanotube occurred due to  $\pi$ - $\pi$  interaction and electrostatic interaction ([Duman et al., 2019](#)).

Since Serp20 was more effective for sulfentrazone adsorption, this material was selected to evaluate the influence of other parameters in the process, such as initial pH and initial concentration. The results are shown in [Figure 8](#).

As can be seen in [Figure 8A](#), the percentage of sulfentrazone removal by Serp20 was greater at acidic pH values, decreasing from 41.7% to 12.7% with an increase in pH from 2 to 10. These results can indicate the participation of cobalt, together with the carbon

structures, in the sulfentrazone removal by a degradation mechanism. Similar behavior was observed in a work with Fe/Ni nanoparticles ([Nascimento et al., 2016](#)). In an acid medium, these particles were able to degrade the sulfentrazone from the aqueous medium by the formation of atomic hydrogen and by direct electron transfer to the herbicide molecule ([Nascimento et al., 2016](#)).

To confirm the degradation of sulfentrazone by  $Co^0$ , alongside the adsorption by carbon structures, experiments were conducted at different pH, and the remaining solutions were analysed by High Performance Liquid Chromatography ([Supplementary Figure S3, ESI†](#)). At pH values 2 and 4, in addition to the sulfentrazone peak with a retention time of 4.84 min, a peak with a retention time of 3.75 min corresponding to a sulfentrazone degradation product was observed. This degradation product, as reported by [Nascimento et al.](#), can be identified as the dechlorinated sulfentrazone molecule ([Nascimento et al., 2016](#)).

Similar results were obtained in other works. [Cruz et al.](#) used  $Co^0/CoO$  nanoparticles for remazol golden yellow dye removal at pH 2 ([Cruz et al., 2019](#)). According to the authors, the electrons from the corrosion of  $Co^0$  can be transferred directly to the dye molecules or for protons present in the system. In the last case, highly reactive hydrogen can induce the cleavage of the azo bond of the dye molecule ([Cruz et al., 2019](#)). [Shao et al.](#) used  $Co^0$  nanoparticles embedded in nitrogen-doped mesoporous carbon nanofibers to promote the hydrogenation of levulinic acid in an  $H_2$  atmosphere. According to the authors, the hydrogenation of levulinic acid occurs due to a reaction with atomic hydrogen, resulting from the dissociation of  $H_2$  adsorbed in  $Co^0$  sites ([Shao et al., 2021](#)).

At pH values above 6, the percentage of removal of sulfentrazone is lower due to the electrostatic repulsion that occurs between Serp20 and sulfentrazone. Besides that, at these pH values, the degradation of the sulfentrazone by  $Co^0$  will not be very significant due to the passivation of the metallic cobalt surface by cobalt oxide. Metallic cobalt is not very stable in an aqueous medium, being oxidized in  $CoO_x$ , which leads to its deactivation during the reaction ([Shao et al., 2021](#)). Acidic conditions promote the removal of a passive layer of oxides and/or hydroxides that form on the metal's surface ([Cruz et al., 2019](#)).

Consequently, we believe that the removal of sulfentrazone occurred by two different mechanisms: adsorption by the carbon species produced in the CVD process and degradation through  $Co^0$  species present in the composites.

The effect of the initial sulfentrazone concentration in the removal process was also investigated. As shown in [Figure 8B](#), with the increase of initial concentration from 5 to 50  $mg L^{-1}$ , the removal efficiency decreased from 53.9% to 14.9%, respectively, due to the occupation of the Serp20 adsorption sites by sulfentrazone.

Since adsorption is the principal removal process of sulfentrazone by Serp20, isotherm assays were performed. The Langmuir and Freundlich isotherm models were adjusted to the experimental data and the results are shown in [Figure 9](#). The parameters of both models can be observed in [Table 1](#).

As can be seen, the Freundlich model fit ( $R^2 = 0.969$ ) was better compared to the Langmuir model fit ( $R^2 = 0.904$ ). The removal capacity obtained experimentally at a sulfentrazone concentration of 50  $mg L^{-1}$  was equal to 14.9  $mg g^{-1}$ .

In other works involving the adsorption of pesticides by carbon-based materials, the Freundlich model was also the one that best fits the experimental data. Essandoh et al. obtained a maximum adsorption capacities for 2,4-dichlorophenoxyacetic acid and 2-methyl-4-chlorophenoxyacetic acid of  $134 \text{ mg g}^{-1}$  and  $50 \text{ mg g}^{-1}$ , respectively, using switchgrass biochar (Essandoh et al., 2017). Liu et al. synthesized a magnetic graphene oxide for neonicotinoid pesticide adsorption getting adsorption capacities ranging from  $1.77\text{--}3.11 \text{ mg g}^{-1}$  (Liu et al., 2017). Suo et al. used P doped biochar from corn straw for the adsorption of triazine achieved a maximum adsorption capacity for atrazine of  $79.6 \text{ mg g}^{-1}$  (Suo et al., 2019).

## 4 Conclusion

In this work, the serpentinite rock ( $\text{Mg}_3\text{SiO}_5(\text{OH})_4$ ) was used as an inorganic matrix for the synthesis of magnetic amphiphilic materials. The serpentinite was impregnated in proportions of 5, 10% and 20% by mass of cobalt/support, to obtain different amounts of carbon nanotubes, since metallic cobalt acts as a catalyst in the formation of multi-walled carbon nanotubes. The CVD process was efficient, and it was obtained 14, 23% and 37% carbon wt, for Serp5, Serp10, and Serp20, respectively. The composites were used for sulfentrazone removal of water and variables such as initial concentration, pH and nature of the adsorbant were studied. The results showed two main mechanisms: adsorption and degradation by Co particles. The removal capacity obtained experimentally at a sulfentrazone concentration of  $50 \text{ mg L}^{-1}$  was equal to  $14.9 \text{ mg g}^{-1}$ .

## Data availability statement

The original contributions presented in the study are included in the article/[Supplementary Material](#), further inquiries can be directed to the corresponding author.

## Author contributions

ED: Conceptualization, Formal Analysis, Methodology, Writing—original draft. AV: Formal Analysis, Methodology, Resources, Writing—review and editing. MN: Formal Analysis, Methodology, Writing—original draft. PP: Writing—original draft. FP: Writing—original draft. RM: Validation, Writing—review and

editing. AT: Funding acquisition, Supervision, Validation, Visualization, Writing—review and editing.

## Funding

The author(s) declare that financial support was received for the research, authorship, and/or publication of this article. CNPq, CAPES, FAPEMIG and INCT MIDAS for financial support UFMG Microscopy Center for the microscopy images. The company Pedras Congonhas for donating of the serpentinite samples. Programa de Produtividade em Pesquisa UEMG (PQ/UEMG 10/2022) for research grant from Paula Sevenini Pinto.

## Acknowledgments

The authors gratefully acknowledge the financial support of CNPq, CAPES, FAPEMIG, INCT MIDAS, and UFMG Microscopy Center. The company Pedras Congonhas for donating of the serpentinite samples. FP thank to Programa de Produtividade em Pesquisa UEMG (PQ/UEMG 10/2022).

## Conflict of interest

The authors declare that the research was conducted in the absence of any commercial or financial relationships that could be construed as a potential conflict of interest.

## Publisher's note

All claims expressed in this article are solely those of the authors and do not necessarily represent those of their affiliated organizations, or those of the publisher, the editors and the reviewers. Any product that may be evaluated in this article, or claim that may be made by its manufacturer, is not guaranteed or endorsed by the publisher.

## Supplementary material

The Supplementary Material for this article can be found online at: <https://www.frontiersin.org/articles/10.3389/frcrb.2024.1402105/full#supplementary-material>

## References

- Alvarez-Silva, M., Uribe-Salas, A., Mirnezami, M., and Finch, J. A. (2010). The point of zero charge of phyllosilicate minerals using the mular-roberts titration technique. *Miner. Eng.* 23 (5), 383–389. doi:10.1016/j.mineng.2009.11.013
- Arepalli, S., Nikolaev, P., Gorelik, O., Hadjiev, V. G., Holmes, W., Files, B., et al. (2004). Protocol for the characterization of single-wall carbon nanotube material quality. *Carbon* 42 (8), 1783–1791. doi:10.1016/j.carbon.2004.03.038
- Ballotin, F. C., Cibaka, T. E., Ribeiro-Santos, T. A., Santos, E. M., Teixeira, A. P. d. C., and Lago, R. M. (2016).  $\text{K}_2\text{MgSiO}_4$ : a novel K<sup>+</sup>-Trapped biodiesel heterogeneous catalyst produced from serpentinite  $\text{Mg}_3\text{Si}_2\text{O}_5(\text{OH})_4$ . *J. Mol. Catal. A Chem.* 422, 258–265. doi:10.1016/j.molcata.2016.02.006
- Cao, C.-Y., Liang, C.-H., Yin, Y., and Du, L.-Yu (2017). Thermal activation of serpentinite for adsorption of cadmium. *J. Hazard. Mater.* 329, 222–229. doi:10.1016/j.jhazmat.2017.01.042
- Chen, T., Fu, C., Liu, Y., Pan, F., Wu, F., You, Z., et al. (2021). Adsorption of volatile organic compounds by mesoporous graphitized carbon: enhanced organophilicity, humidity resistance, and mass transfer. *Sep. Purif. Technol.* 264, 118464. doi:10.1016/j.seppur.2021.118464
- Cruz, J. C., Nascimento, M. A., Amaral, H. A. V., Lima, D. S. D., Teixeira, A. P. C., and Lopes, R. P. (2019). Synthesis and characterization of cobalt nanoparticles for application in the removal of textile dye. *J. Environ. Manag.* 242, 220–228. doi:10.1016/j.jenvman.2019.04.059

- Dresselhaus, G., Avouris, P., and Dresselhaus, M. S. (2001) *Carbon nanotubes: synthesis, structure, properties, and applications*. Berlin, Heidelberg: Springer. doi:10.1007/3-540-39947-X
- Drizo, A., Forget, C., Chapuis, R. P., and Comeau, Y. (2006). Phosphorus removal by electric arc furnace steel slag and serpentinite. *Water Res.* 40, 1547–1554. doi:10.1016/j.watres.2006.02.001
- Duman, O., Özcan, C., Gürkan Polat, T., and Tunç, S. (2019). Carbon nanotube-based magnetic and non-magnetic adsorbents for the high-efficiency removal of diquat dibromide herbicide from water: OMWCNT, OMWCNT-Fe<sub>3</sub>O<sub>4</sub> and OMWCNT-κ-carrageenan-Fe<sub>3</sub>O<sub>4</sub> nanocomposites. *Environ. Pollut.* 244, 723–732. doi:10.1016/j.envpol.2018.10.071
- Dupuis, A.-C. (2005). The catalyst in the CCVD of carbon nanotubes—a review. *Prog. Mater. Sci.* 50 (8), 929–961. doi:10.1016/j.pmatsci.2005.04.003
- Essandoh, M., Wolgemuth, D., Pittman, C. U., Mohan, D., and Mlsna, T. (2017). Phenox herbicide removal from aqueous solutions using fast pyrolysis switchgrass biochar. *Chemosphere* 174, 49–57. doi:10.1016/j.chemosphere.2017.01.105
- Hirth, G., and Guillot, S. (2013). Rheology and tectonic significance of serpentinite. *Elements* 9 (2), 107–113. doi:10.2113/gselements.9.2.107
- Lelario, F., Gardi, I., Mishael, Y., Dolev, N., Undabeytia, T., Nir, S., et al. (2017). Pairing micropollutants and clay-composite sorbents for efficient water treatment: filtration and modeling at a pilot scale. *Appl. Clay Sci.* 137, 225–232. doi:10.1016/j.clay.2016.12.029
- Lemos, B. R. S., Soares, Ê. A. R., Teixeira, A. P. C., Ardisson, J. D., Fernandez-Outon, L. E., Amorim, C. C., et al. (2016). Growth of carbon structures on chrysotile surface for organic contaminants removal from wastewater. *Chemosphere* 159, 602–609. doi:10.1016/j.chemosphere.2016.06.022
- Liu, G., Li, L., Xu, D., Huang, X., Xu, X., Zheng, S., et al. (2017). Metal–organic framework preparation using magnetic graphene oxide-β-cyclodextrin for neonicotinoid pesticide adsorption and removal. *Carbohydr. Polym.* 175, 584–591. doi:10.1016/j.carbpol.2017.06.074
- Martinez, C. O., Silva, C. M. M. S., Fay, E. F., Nunesmaia, A., Abakerli, R. B., and Durrant, L. R. (2008). Degradation of the herbicide sulfentrazone in a Brazilian typical hapludox soil. *Soil Biol. Biochem.* 40 (4), 879–886. doi:10.1016/j.soilbio.2007.10.016
- McKee, G. S. B., and Vecchio, K. S. (2006). Thermogravimetric analysis of synthesis variation effects on CVD generated multiwalled carbon nanotubes. *J. Phys. Chem. B* 110 (3), 1179–1186. doi:10.1021/jp054265h
- Momčilović, M. Z., Randelović, M. S., Purenović, M. M., Đorđević, J. S., Onjia, A., and Matović, B. (2016). Morpho-structural, adsorption and electrochemical characteristics of serpentinite. *Sep. Purif. Technol.* 163, 72–78. doi:10.1016/j.seppur.2016.02.042
- Montoro, L. A., Corio, P., and Rosolen, J. M. (2007). A comparative study of alcohols and ketones as carbon precursor for multi-walled carbon nanotube growth. *Carbon* 45 (6), 1234–1241. doi:10.1016/j.carbon.2007.01.025
- Nascimento, M. A., Lopes, R. P., Cruz, J. C., Silva, A. A., and Lima, C. F. (2016). Sulfentrazone dechlorination by iron-nickel bimetallic nanoparticles. *Environ. Pollut.* 211, 406–413. doi:10.1016/j.envpol.2015.12.043
- O’Connell, M. J., and O’Connell, M. J. (2006) *Carbon nanotubes: properties and applications*. Boca Raton City Taylor and Francis Group, LLC.
- Öncel, Ç., and Yürüm, Y. (2006). Carbon nanotube synthesis via the catalytic CVD method: a review on the effect of reaction parameters. *Fullerenes, Nanotub. Carbon Nanostructures* 14 (1), 17–37. doi:10.1080/15363830500538441
- Pimenta, M. A., Dresselhaus, G., Dresselhaus, M. S., Cancado, L. G., Jorio, A., and Saito, R. (2007). Studying disorder in graphite-based systems by Raman spectroscopy. *Phys. Chem. Chem. Phys.* 9 (11), 1276–1290. doi:10.1039/B613962K
- Purceno, A. D., Barriani, B. R., Dias, A., da Costa, G. M., Lago, R. M., and Moura, F. C. C. (2011). Carbon nanostructures-modified expanded vermiculites produced by chemical vapor deposition from ethanol. *Appl. Clay Sci.* 54 (1), 15–19. doi:10.1016/j.clay.2011.06.012
- Purceno, A. D., Teixeira, A. P. C., Souza, N. J. d., Fernandez-Outon, L. E., Ardisson, J. D., and Lago, R. M. (2012). Hybrid magnetic amphiphilic composites based on carbon nanotube/nanofibers and layered silicates fragments as efficient adsorbent for ethyniletriadrol. *J. Colloid Interface Sci.* 379 (1), 84–88. doi:10.1016/j.jcis.2012.04.018
- Rodrigues, B. N., and Sousa de Almeida, F. (2018) *Guia de Herbicidas*. 7th ed. Viçosa city Produção Independente.
- Shao, S., Yang, Y., Guo, S., Hao, S., Yang, F., Zhang, S., et al. (2021). Highly active and stable Co nanoparticles embedded in nitrogen-doped mesoporous carbon nanofibers for aqueous-phase levulinic acid hydrogenation. *Green Energy and Environ.* 6 (4), 567–577. doi:10.1016/j.gee.2020.11.005
- Siqueira, S. L. de, and Kruse, M. H. L. (2008). Agrotóxicos e Saúde Humana: Contribuição Dos Profissionais Do Campo Da Saúde. *Rev. Esc. Enferm. USP* 42, 584–590. doi:10.1590/s0080-62342008000300024
- Suo, F., You, X., Ma, Y., and Li, Y. (2019). Rapid removal of triazine pesticides by P doped biochar and the adsorption mechanism. *Chemosphere* 235, 918–925. doi:10.1016/j.chemosphere.2019.06.158
- Teixeira, A. P. C., Purceno, A. D., Barros, A. S., Lemos, B. R. S., Ardisson, J. D., Macedo, W. A. A., et al. (2012). Amphiphilic magnetic composites based on layered vermiculite and fibrous chrysotile with carbon nanostructures: application in catalysis. *Catal. Today* 190 (1), 133–143. doi:10.1016/j.cattod.2012.01.042
- Teixeira, A. P. C., Purceno, A. D., de Paula, C. C. A., da Silva, J. C. C., Ardisson, J. D., and Lago, R. M. (2013). Efficient and versatile fibrous adsorbent based on magnetic amphiphilic composites of chrysotile/carbon nanostructures for the removal of ethyniletriadrol. *J. Hazard. Mater.* 248–249 (249), 295–302. doi:10.1016/j.jhazmat.2013.01.014
- Undabeytia, T., Nir, S., Sánchez-Verdejo, T., Villaverde, J., Maqueda, C., and Morillo, E. (2008). A clay–vesicle system for water purification from organic pollutants. *Water Res.* 42 (4), 1211–1219. doi:10.1016/j.watres.2007.09.004
- Yang, W., Sun, W. J., Chu, W., Jiang, C.F., and Wen, J. (2012). Synthesis of carbon nanotubes using scrap tyre rubber as carbon source. *Chin. Chem. Lett.* 23 (3), 363–366. doi:10.1016/j.ccl.2012.01.006
- Zhao, W., Lee, Mi J., Kim, H. T., and Kim, Ik J. (2011). The synthesis of carbon nanotubes (CNTs) by catalytic CVD using a Fe/Co-supported zeolite template. *Electron. Mater. Lett.* 7 (2), 139–144. doi:10.1007/s13391-011-0609-6